



Supporting Information

Probing the Origin of Viscosity of Liquid Electrolytes for Lithium Batteries

N. Yao, L. Yu, Z.-H. Fu, X. Shen, T.-Z. Hou, X. Liu, Y.-C. Gao, R. Zhang, C.-Z. Zhao,
X. Chen*, Q. Zhang*

SUPPORTING INFORMATION

Experimental Procedures

1.1 Molecular dynamics simulations.

Molecular dynamics (MD) simulations were performed using LAMMPS (Ver. 29 Sep 2021).^[1] Constructed models of solvents and electrolytes are listed in Supplementary Table 4. The solvent force field parameters were generated by the LigParGen web server^[2] using the OPLS-AA^[3] force field due to that it is widely applied in organic liquids and electrolyte simulations,^[4] and the study by Park *et al.*^[5] showed that OPLS-AA performed better than other tested force fields in calculating viscosity. Besides, advanced restrained electrostatic potential (RESP2) atomic partial charges were adopted, which were derived from the electrostatic potential (ESP) charges using the Multiwfn program (Ver. 3.7).^[6] The parameters for Li⁺ and FSI⁻ were obtained from Jensen *et al.*^[7] and Lopes *et al.*,^[8] respectively. The initial atomic coordinates were generated by PACKMOL (Ver. 20.010),^[9] and the MD snapshots were visualized by VESTA (Ver. 3.5.7).^[10]

Five parallel simulations were conducted for each system in Supplementary Table 4. The time step was fixed to be 1 fs for all simulations. All systems were first equilibrated in the isothermal–isobaric (constant NPT) ensemble using the Parrinello–Rahman barostat^[11] for 1 ns to maintain a temperature of 298 K (315 K for EC-containing systems) and a pressure of 1 atm with time constants of 0.1 and 1 ps, respectively. Subsequently, the systems were heated from 298 or 315 to 400 K within 0.5 ns and maintained at 400 K for 0.5 ns, followed by annealing from 400 to 298 or 315 K within 0.5 ns. After that, all systems were equilibrated at 298 or 315 K in a constant NPT ensemble for another 1 ns. A production run of 20 ns at 298 K in the canonical (constant NVT) ensemble under Nose–Hoover thermostat^[12] was finally conducted, which was used to compute viscosity. The relative errors (δ) of computed viscosities (η_{cal}) with respect to experimental values (η_{exp}) are determined as follows:

$$\delta = \frac{\eta_{\text{cal}} - \eta_{\text{exp}}}{\eta_{\text{exp}}} \times 100\% \quad (\text{S1})$$

The diffusion coefficients (D) were calculated by the Python package MDAnalysis^[13] according to the Einstein relation:

$$D = \lim_{t \rightarrow \infty} \left[\frac{1}{2dt} \text{MSD}(t) \right] \quad (\text{S2})$$

$$\text{MSD}(t) = \frac{1}{N} \sum_{i=1}^N \langle [\mathbf{r}_i(t)]^2 \rangle = \frac{1}{N} \sum_{i=1}^N \frac{1}{N_t} \sum_{t_0=0}^{t_{\text{tot}}-t} |\mathbf{r}_i(t_0 + t) - \mathbf{r}_i(t_0)|^2 \quad (\text{S3})$$

where d , N , and $\mathbf{r}_i(t)$ denote the diffusion dimension, the number of the diffusing ions, and the displacement of atom i after time t , respectively. The MSD is averaged over all possible time intervals t to maximize the number of samples. D is known to have finite-size effects,^[5, 14] and therefore D of solvents and ions in three DMC/LiFSI electrolytes with low (LC, 1.1 M), moderate (MC, 3.1 M), and high (HC, 4.9 M) salt concentrations were evaluated in different simulation box sizes (Figure S12c). D are system-size dependent at the initial increase of the box size due to distinct effects caused by hydrodynamic interactions.^[14] Hydrodynamic interactions then decay with the further increase of the box size and are no longer competitive compared to electrostatic interactions which are strong in considered electrolyte systems, leading to the convergence of D . And most important, the trend that D of solvents and ions decrease with increasing salt concentrations remains despite finite size effects of D , and hence the smallest model size was adopted for the sake of simulation efficiency.

The solvation structures were analyzed based on the Python package MDTraj^[15] by traversing 5000 frames that were output every 1 ps during the last 5 ns simulations. The respective numbers of clusters with different sizes can be counted for each frame and then added up for all 5000 frames. Dividing the number of clusters with a certain size by the sum of all clusters gives the corresponding proportion.

1.2 Calculation of the binding energy.

For pure solvents, the binding energy (E_b) between molecules was defined as the energy difference between the molecule in solution (E_{sol}) and vacuum (E_{vac}):

$$E_b = E_{\text{sol}} - E_{\text{vac}} \quad (\text{S4})$$

where E_{sol} is the average energy of a solvent in the simulation system with 200 molecules. The mean and variance values of E_{sol} were calculated over total 20,000 energy values that were output every 1 ps during the 20 ns NVT production run. Two hundred molecular configurations were randomly extracted from the simulation trajectory, and the single point energy of each configuration was calculated by MD simulations to obtain the mean and variance values of E_{vac} . The standard deviation of E_b is the square root of the sum of variances of E_{sol} and E_{vac} supposing these two sets of data are not correlated and thus the covariance equals zero.

For binary solvent mixtures, the binding energy between molecules was defined similarly:

$$E_b = E_{\text{sol}} - (1-x)E_{\text{vac},1} - xE_{\text{vac},2} \quad (\text{S5})$$

where $(1-x)$ and x are the molar fractions of individual solvent components. E_{sol} here is the average energy of a solvent in the simulation system with 400 molecules.

In electrolyte systems, ion solvation takes place, and this was taken into consideration when defining the binding energy of electrolytes:

$$E_b = \frac{E_{\text{tot}} - (N_{\text{Solvent}} \times E_{\text{Solvent}} + N_{\text{Li}^+} \times E_{\text{Li}^+} + N_{\text{FSI}^-} \times E_{\text{FSI}^-})}{N_{\text{Solvent}} + N_{\text{Li}^+} + N_{\text{FSI}^-}} \quad (\text{S6})$$

$$E_{\text{Li}^+} = E_{\text{Li}^{+, \text{free}}} + \frac{1}{2} \times \text{CN}_{\text{FSI}^-} \times E_{\text{b,Li}^+-\text{FSI}^-} \quad (\text{S7})$$

$$E_{\text{FSI}^-} = E_{\text{FSI}^{-, \text{free}}} + \frac{1}{2} \times E_{\text{b,Li}^+-\text{FSI}^-} \quad (\text{S8})$$

where N is the number of corresponding ions or molecules and CN_{FSI^-} the average coordination number of FSI⁻ around Li⁺.

SUPPORTING INFORMATION

Supporting Figures

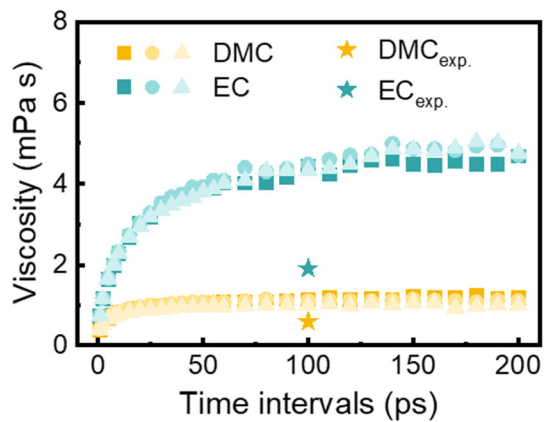


Figure S1. The viscosity convergence of DMC and EC solvents with increasing time intervals.

SUPPORTING INFORMATION

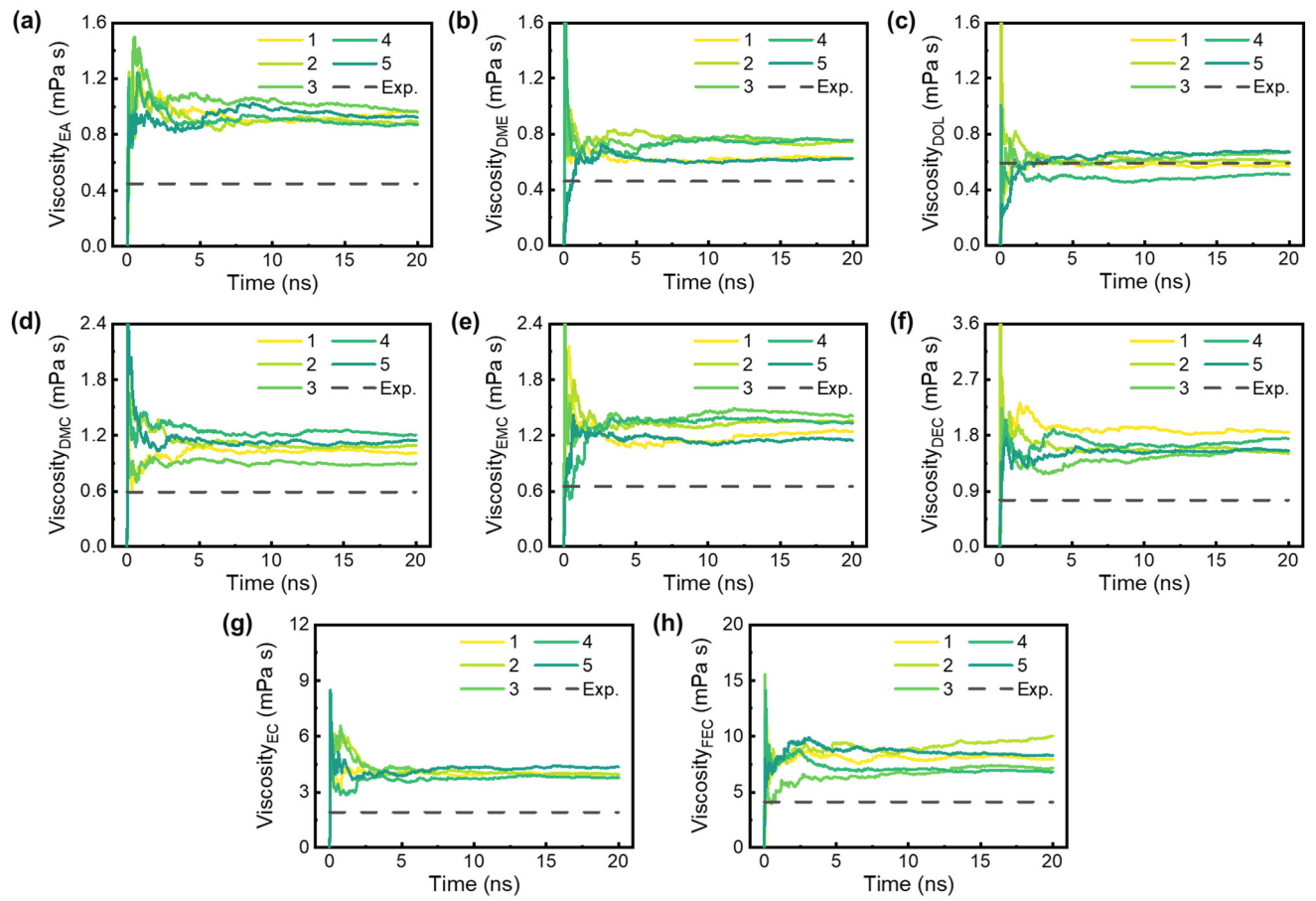


Figure S2. The viscosities of (a) EA, (b) DME, (c) DOL, (d) DMC, (e) EMC, (f) DEC, (g) EC, and (h) FEC calculated by the splitting method (SM).

SUPPORTING INFORMATION

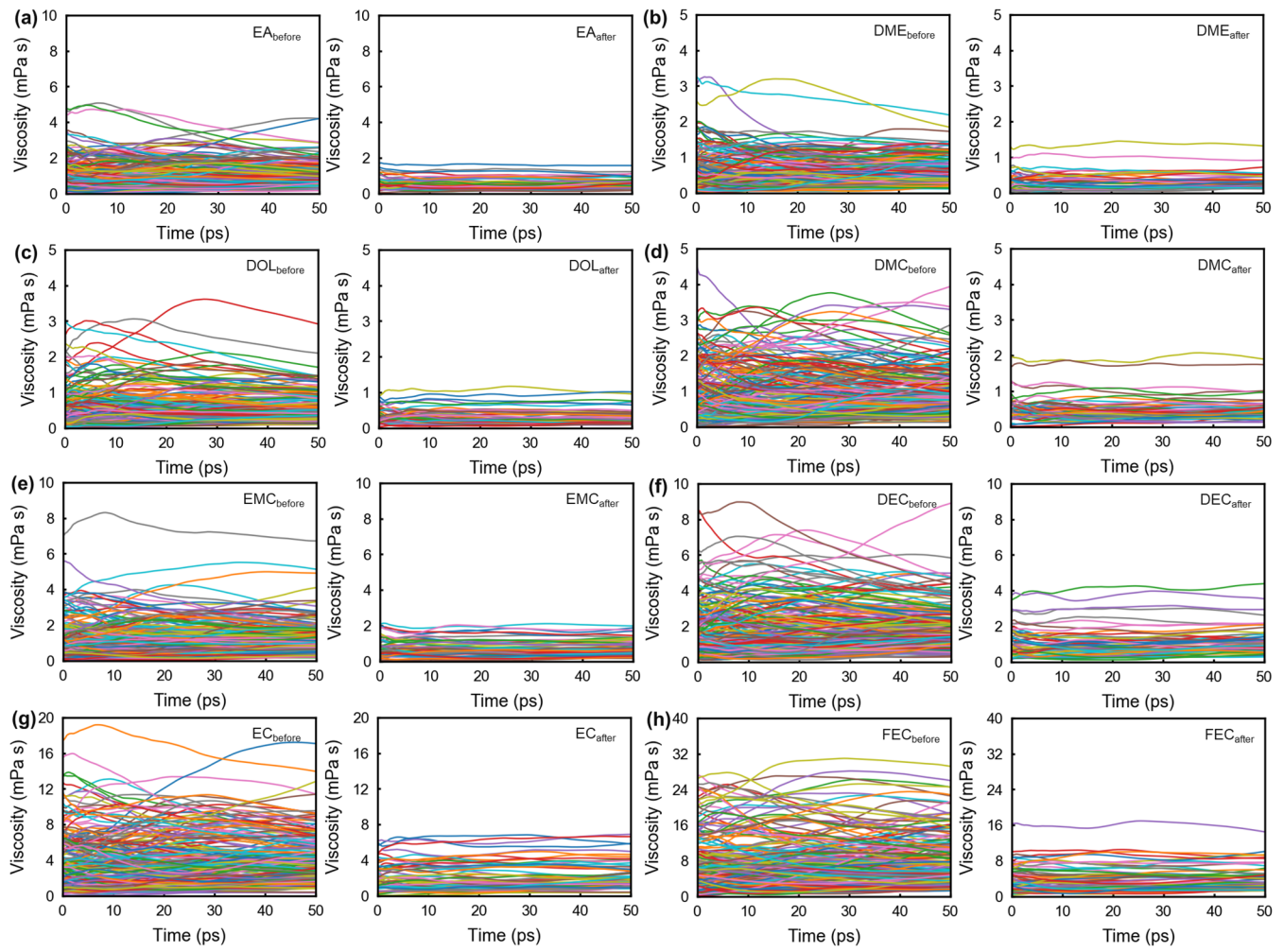


Figure S3. The viscosities of samples for (a) EA, (b) DME, (c) DOL, (d) DMC, (e) EMC, (f) DEC, (g) EC, and (h) FEC computed by the overlapping method (OM) and after setting the standard deviation (std) threshold to screen divergent samples.

SUPPORTING INFORMATION

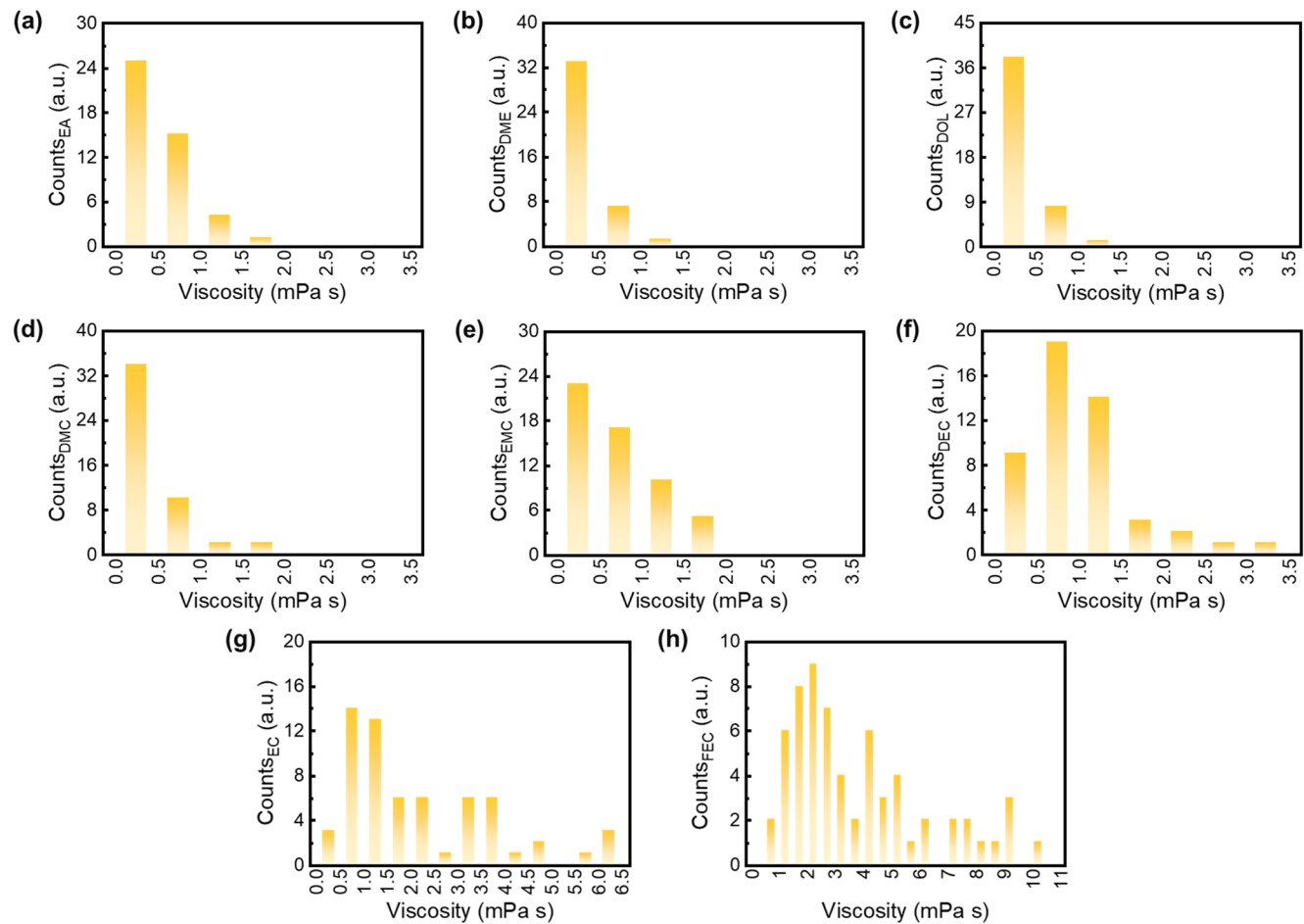


Figure S4. The distribution of viscosity values of (a) EA, (b) DME, (c) DOL, (d) DMC, (e) EMC, (f) DEC, (g) EC, and (h) FEC solvents after setting the std threshold to screen divergent samples.

SUPPORTING INFORMATION

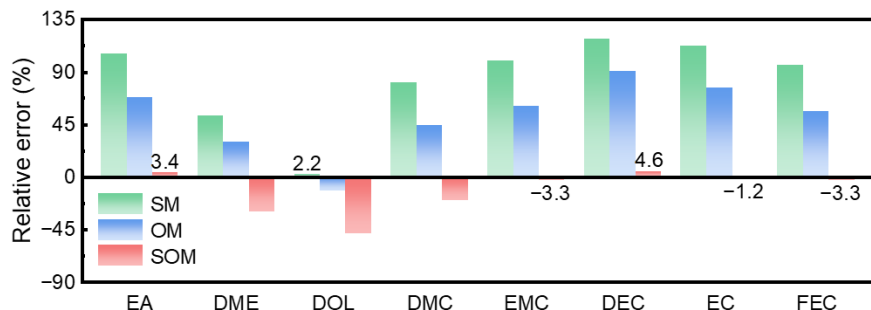


Figure S5. The comparison of relative errors of viscosities computed by SM, OM, and SOM with respect to experimental values.

SUPPORTING INFORMATION

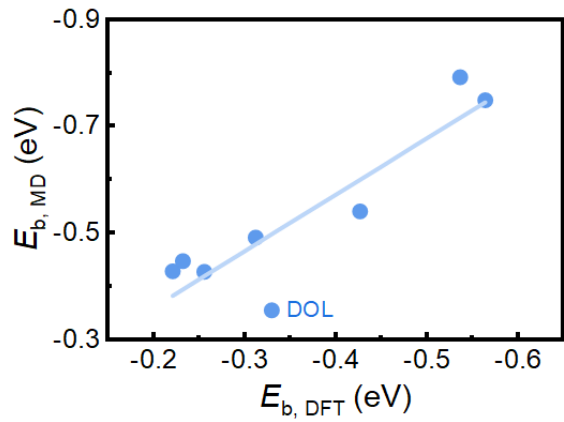


Figure S6. The binding energies calculated by the MD simulation and high-accuracy density functional theory calculation.

SUPPORTING INFORMATION

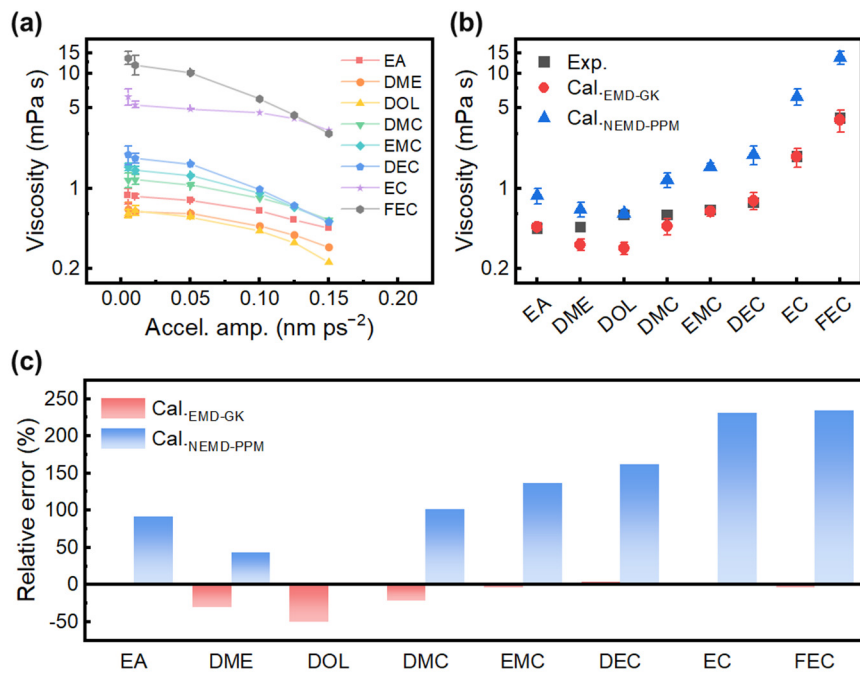


Figure S7. The comparison of viscosities computed by SOM (EMD-GK) and nonequilibrium MD-based periodic perturbation method (NEMD-PPM) with respect to experimental values. (a) The convergence of NEMD-PPM viscosities with the applied acceleration amplitudes. The (b) viscosities and (c) the relative errors of viscosities of EMD-GK and NEMD-PPM.

SUPPORTING INFORMATION

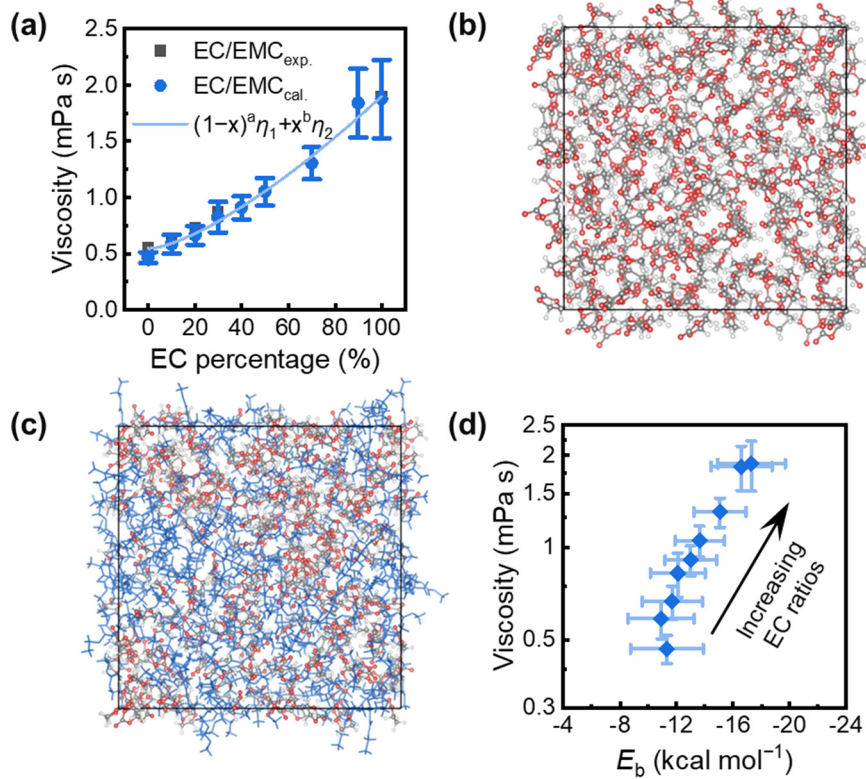


Figure S8. The viscosities and binding energies of EC/EMC binary solvent mixtures with different mixing ratios. (a) The computed and experimental^[16] viscosities of EC/EMC mixtures with varied EC molar percentages. The MD snapshot of (b) pure EC solvents and (c) EC/EMC mixtures with a molar ratio of 1:1. EC molecules are represented by colored ball sticks while EMC molecules are represented by green sticks. Color mapping for elements: H-white, C-gray, O-red. (d) The correlation between the viscosities and binding energies in EC/EMC mixtures.

SUPPORTING INFORMATION

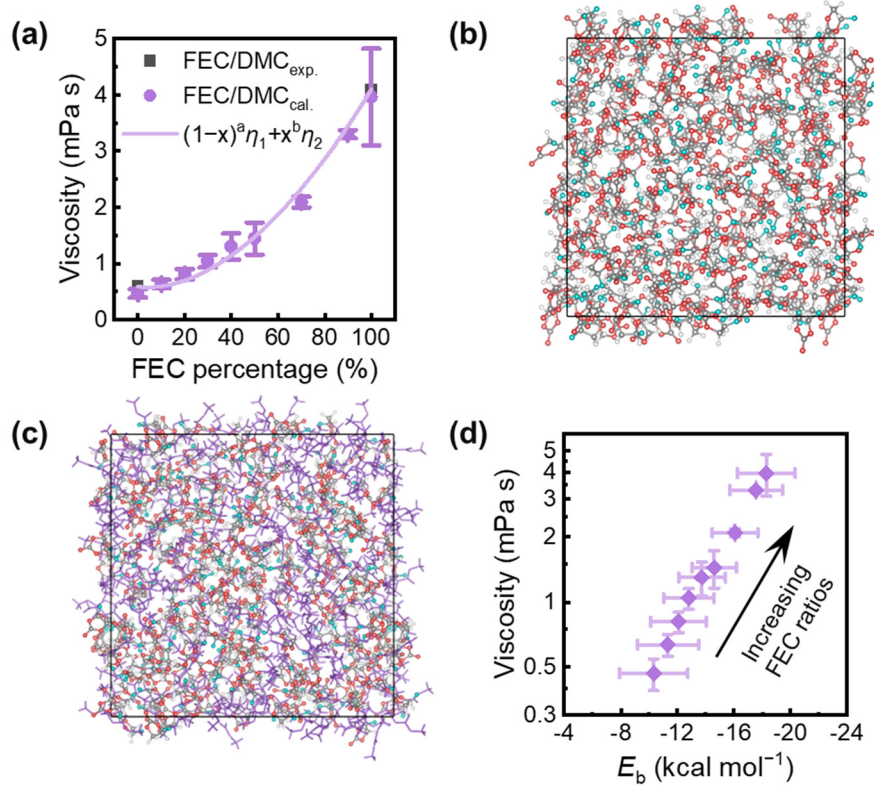


Figure S9. The viscosities and binding energies of FEC/DMC binary solvent mixtures with different mixing ratios. (a) The viscosities of FEC/DMC mixtures with varied FEC molar percentages. The MD snapshot of (b) pure FEC solvents and (c) FEC/DMC mixtures with a molar ratio of 1:1. FEC molecules are represented by colored ball sticks while DMC molecules are represented by green sticks. Color mapping for elements: H-white, C-gray, O-red, F-cyan. (d) The correlation between the viscosities and binding energies in FEC/DMC mixtures.

SUPPORTING INFORMATION

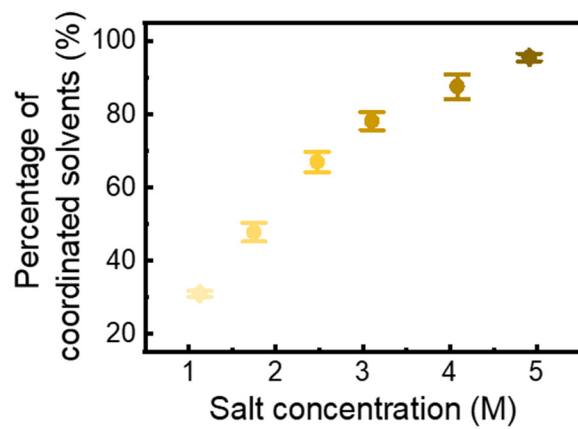


Figure S10. The change of the percentage of solvents in Li^+ solvation shells as the salt concentration increases.

SUPPORTING INFORMATION

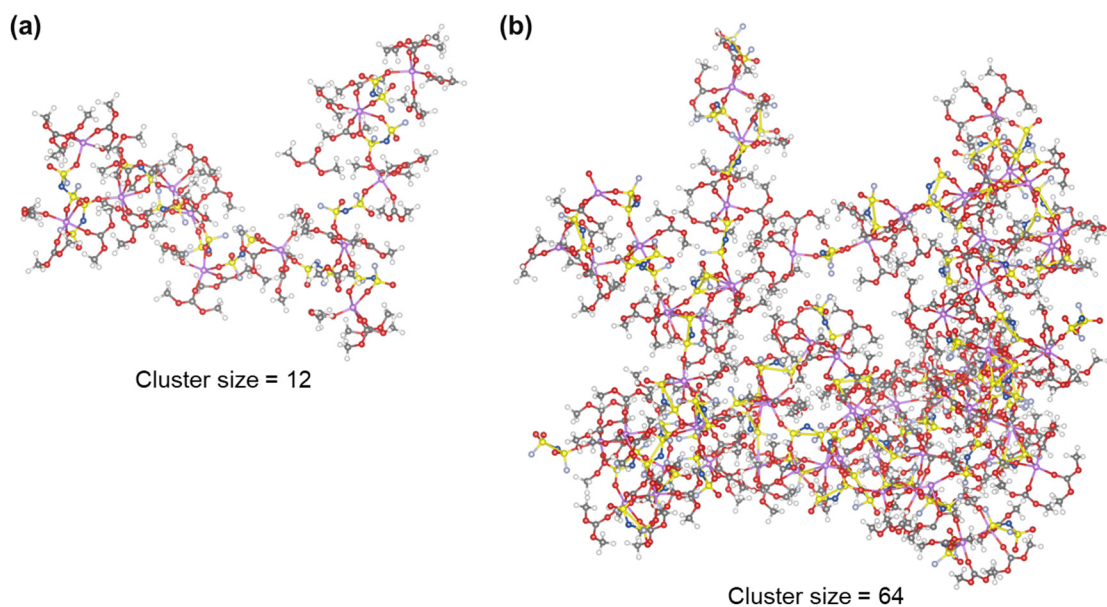


Figure S11. The extracted solvation structures with cluster sizes of (a) 12 and (b) 64, where the cluster size is defined as the number of Li^+ in isolated $\text{Li}^+ \text{FSI}^- \text{DMC}$ clusters. Color mapping for elements: H-white, Li-violet, C-gray, N-blue, O-red, F-light purple, S-yellow.

SUPPORTING INFORMATION

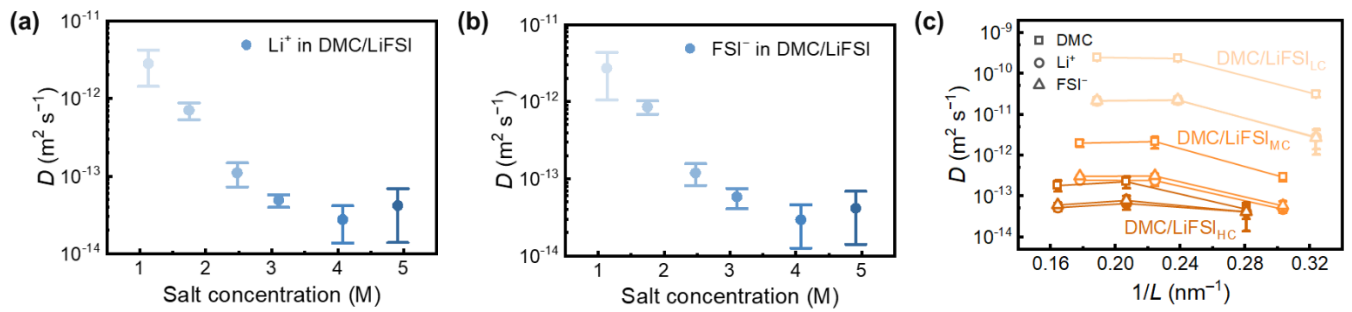


Figure S12. The diffusion coefficients (D) of (a) Li^+ and (b) FSI^- in DMC/LiFSI electrolytes with different salt concentrations, and (c) Li^+ , FSI^- , and DMC in three electrolytes with low (LC, 1.1 M), moderate (MC, 3.1 M), and high (HC, 4.9 M) salt concentrations in different simulation box sizes (L). The trend that D of solvents and ions decrease with increasing salt concentrations remains despite finite size effects of D . Detailed discussion have been stated in the Method part.

SUPPORTING INFORMATION

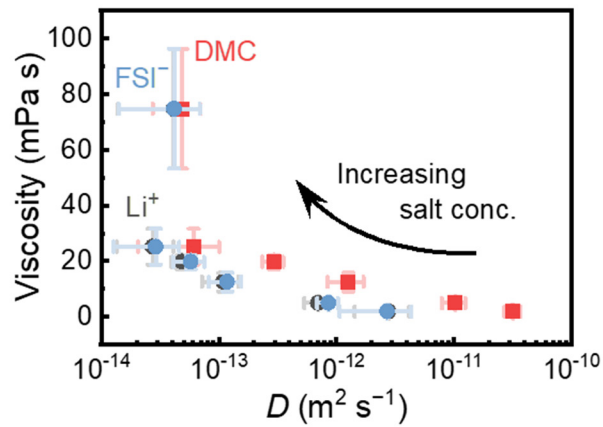


Figure S13. The correlation between diffusion coefficients (D) of particles in DMC/LiFSI electrolytes and viscosities of electrolytes with different salt concentrations.

SUPPORTING INFORMATION

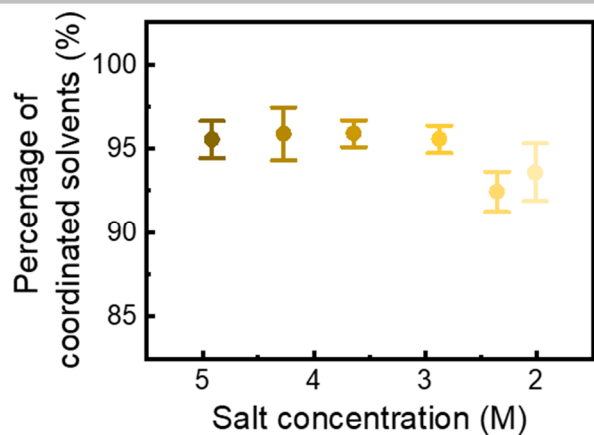


Figure S14. The change of the percentage of solvents in Li^+ solvation shells in electrolytes with different diluent ratios, *i.e.*, different salt concentrations.

SUPPORTING INFORMATION

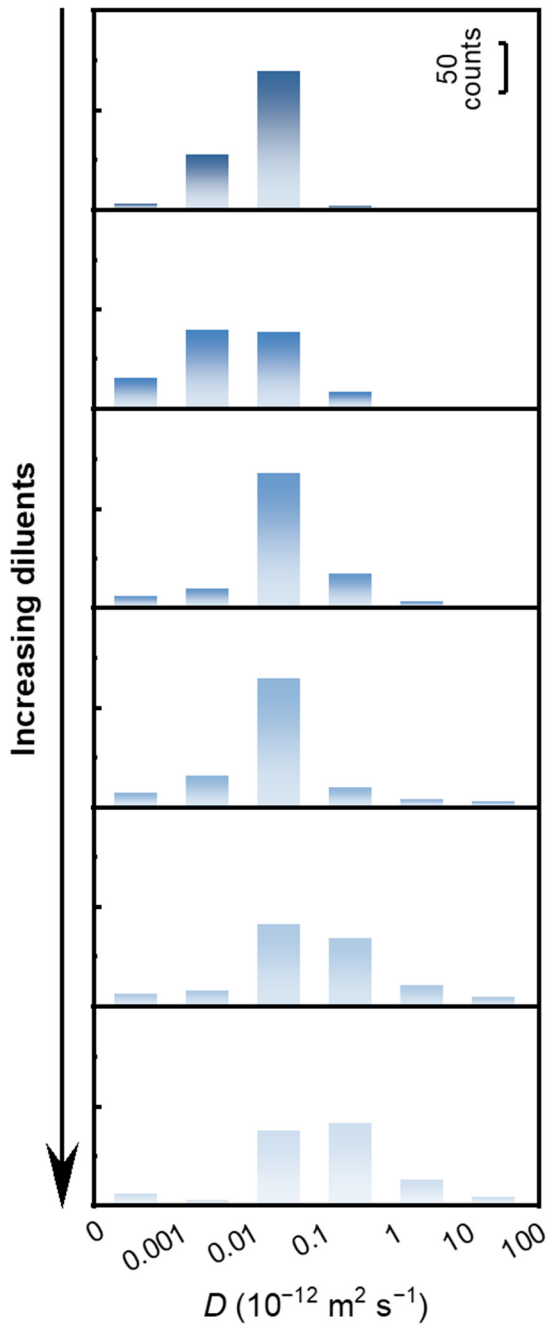


Figure S15. The distribution of the diffusion coefficients (D) of each DMC molecule in electrolytes with different diluent ratios, *i.e.*, different salt concentrations.

SUPPORTING INFORMATION

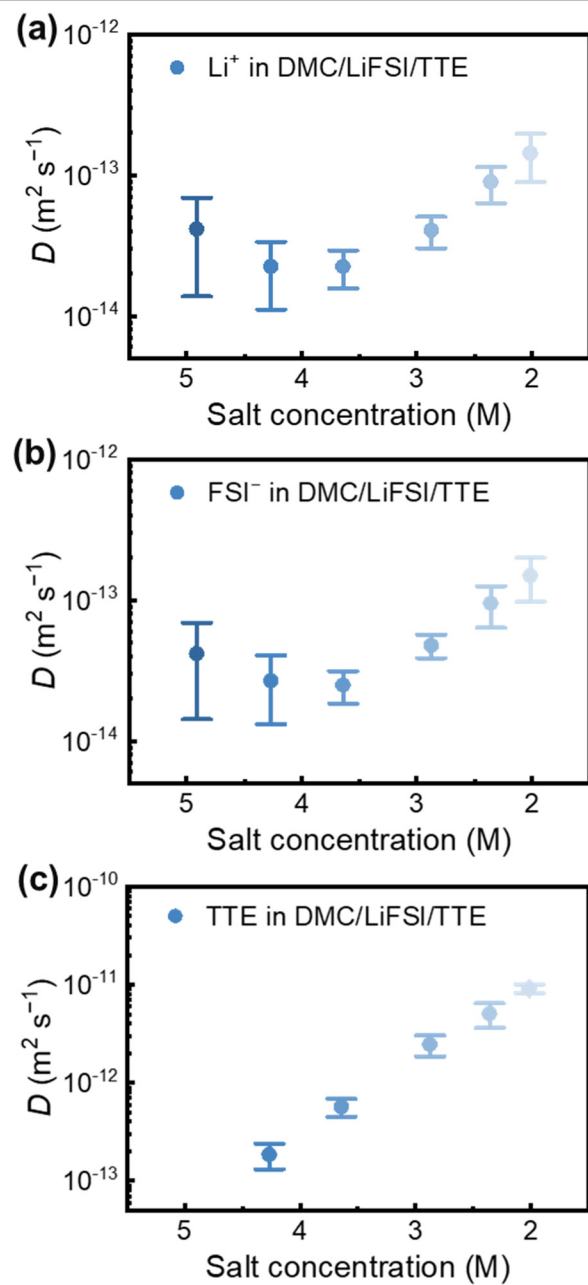


Figure S16. The diffusion coefficients (D) of (a) Li^+ , (b) FSI^- , and (c) TTE in DMC/LiFSI/TTE electrolytes with different diluent ratios, i.e., different salt concentrations.

SUPPORTING INFORMATION

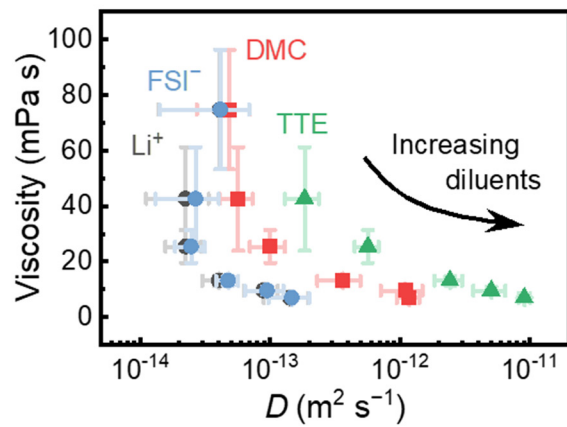


Figure S17. The correlation between diffusion coefficients (D) of particles in DMC/LiFSI/TTE electrolytes and viscosities of electrolytes with different diluent ratios, *i.e.*, different salt concentrations.

SUPPORTING INFORMATION

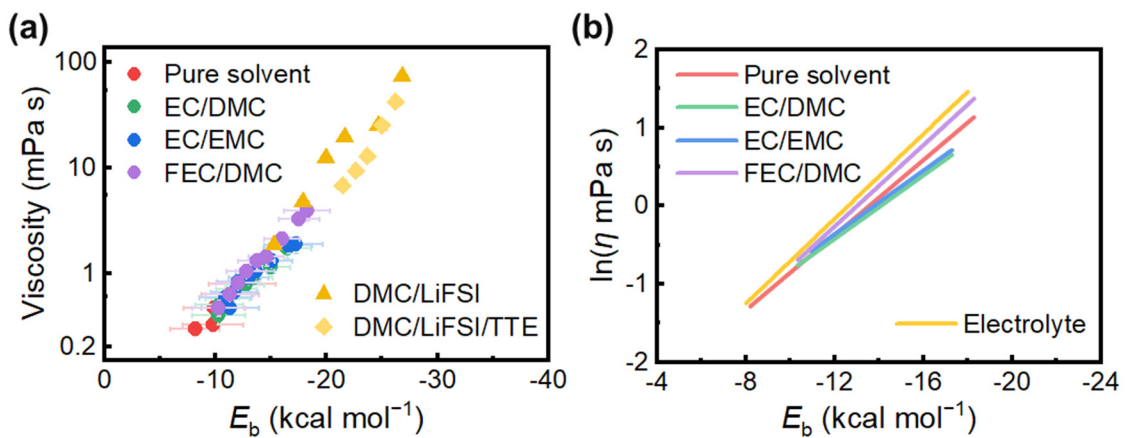


Figure S18. The correlation between the binding energy and viscosity of pure solvents, solvent mixtures, and electrolytes.

SUPPORTING INFORMATION

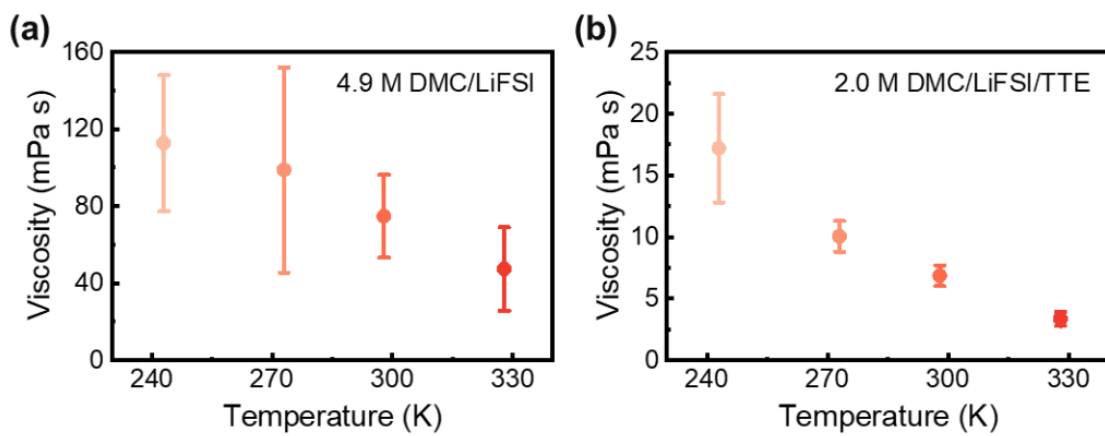


Figure S19. The temperature dependence of viscosities of (a) 4.9 M DMC/LiFSI and (b) 2.0 M DMC/LiFSI/TTE.

SUPPORTING INFORMATION**Supporting Tables****Table S1.** The pre-exponential (A) and exponent (α) fitting parameters of the correlation between the binding energy and viscosity.

System	$\ln(A \text{ mPa s})$	α
Pure solvent	-3.25	7.02
EC/DMC	-2.86	8.43
EC/EMC	-2.80	8.43
FEC/DMC	-3.38	6.48
Electrolyte	-3.42	6.25

SUPPORTING INFORMATION**Table S2.** The fitting parameters a and b of the viscosity of solvent mixtures.

System	a	b
EC/DMC	1.54	1.36
EC/EMC	1.00	1.28
FEC/DMC	1.14	1.76

SUPPORTING INFORMATION**Table S3.** The viscosities of pure solvents calculated based on the equation of the viscosity of an ideal gas.

System	Diameter (Å)	Viscosity (mPa s)
EA	8.06	0.0057
DME	8.06	0.0046
DOL	7.24	0.0051
DMC	7.62	0.0051
EMC	8.02	0.0050
DEC	8.42	0.0048
EC	7.34	0.0055
FEC	7.44	0.0058

SUPPORTING INFORMATION

Table S4. The number of constituents in MD simulation models.

System	Solvent 1	Solvent 2	Salt	Diluent	Conc. (M)
Pure solvent	200				
Solvent mixture	200	200			
			20		1.1
			33		1.7
DMC/LiFSI	200		50		2.5
			67		3.1
			100		4.1
			133		4.9
DMC/LiFSI/TTE	200		133	27	4.3
				67	3.6
				133	2.9
				200	2.4
				267	2.0

SUPPORTING INFORMATION

References

- [1] P. Steve, *J. Comput. Phys.* **1995**, *117*, 1–19.
- [2] L. S. Doddà, I. C. de Vaca, J. Tirado-Rives, W. L. Jorgensen, *Nucleic Acids Res.* **2017**, *45*, W331–W336.
- [3] W. L. Jorgensen, D. S. Maxwell, J. Tirado-Rives, *J. Am. Chem. Soc.* **1996**, *118*, 11225–11236.
- [4] Q. Li, S. Tan, L. Li, Y. Lu, Y. He, *Sci. Adv.* **2017**, *3*, e1701246; Z. Yu, H. Wang, X. Kong, W. Huang, Y. Tsao, D. G. Mackanic, K. Wang, X. Wang, W. Huang, S. Choudhury, Y. Zheng, C. V. Amanchukwu, S. T. Hung, Y. Ma, E. G. Lomeli, J. Qin, Y. Cui, Z. Bao, *Nat. Energy* **2020**, *5*, 526–533; J. Holoubek, H. Liu, Z. Wu, Y. Yin, X. Xing, G. Cai, S. Yu, H. Zhou, T. A. Pascal, Z. Chen, P. Liu, *Nat. Energy* **2021**, *6*, 303–313; F. Chen, X. Wang, M. Armand, M. Forsyth, *Nat. Mater.* **2022**, *21*, 1175–1182; Z. Yu, P. E. Rudnicki, Z. Zhang, Z. Huang, H. Celik, S. T. Oyakhire, Y. Chen, X. Kong, S. C. Kim, X. Xiao, H. Wang, Y. Zheng, G. A. Kamat, M. S. Kim, S. F. Bent, J. Qin, Y. Cui, Z. Bao, *Nat. Energy* **2022**, *7*, 94–106; N. Yao, X. Chen, Z.-H. Fu, Q. Zhang, *Chem. Rev.* **2022**, *122*, 10970–11021.
- [5] C. Park, M. Kanduč, R. Chudoba, A. Ronneburg, S. Risso, M. Ballauff, J. Dzubiella, *J. Power Sources* **2018**, *373*, 70–78.
- [6] T. Lu, F.-W. Chen, *J. Comput. Chem.* **2012**, *33*, 580–592.
- [7] K. P. Jensen, W. L. Jorgensen, *J. Chem. Theory Comput.* **2006**, *2*, 1499–1509.
- [8] J. N. Canongia Lopes, K. Shimizu, A. A. H. Pádua, Y. Umebayashi, S. Fukuda, K. Fujii, S.-i. Ishiguro, *J. Phys. Chem. B* **2008**, *112*, 9449–9455.
- [9] L. Martinez, R. Andrade, E. G. Birgin, J. M. Martinez, *J. Comput. Chem.* **2009**, *30*, 2157–2164.
- [10] K. Momma, F. Izumi, *J. Appl. Crystallogr.* **2011**, *44*, 1272–1276.
- [11] M. Parrinello, A. Rahman, *J. Appl. Phys.* **1981**, *52*, 7182–7190.
- [12] W. G. Hoover, *Phys. Rev. A* **1985**, *31*, 1695–1697; S. Nose, *Mol. Phys.* **1984**, *52*, 255–268.
- [13] N. Michaud-Agrawal, E. J. Denning, T. B. Woolf, O. Beckstein, *J. Comput. Chem.* **2011**, *32*, 2319–2327.
- [14] I.-C. Yeh, G. Hummer, *J. Phys. Chem. B* **2004**, *108*, 15873–15879.
- [15] R. T. McGibbon, K. A. Beauchamp, M. P. Harrigan, C. Klein, J. M. Swails, C. X. Hernandez, C. R. Schwantes, L.-P. Wang, T. J. Lane, V. S. Pande, *Biophys. J.* **2015**, *109*, 1528–1532.
- [16] E. R. Logan, E. M. Tonita, K. L. Gering, L. Ma, M. K. G. Bauer, J. Li, L. Y. Beaulieu, J. R. Dahn, *J. Electrochem. Soc.* **2018**, *165*, A705–A716.